Pak. J. Chem. 16(1-2): 38-44, 2026 Research article
ISSN (Print): 2220-2625
ISSN (Online): 2222-307X DOI: 10.15228/2026.v16.i1-2.p05

Laser Induced Breakdown Spectroscopy for Elemental Profiling and Plasma Diagnostics of Cosmetic Products

Saifullah Jamali[1,2]*, Nek Muhammad Shaikh[1], Zhirong Zhang[2], Hongbo Fu[2], Waseem Ahmed Bhutto[1], Abdul Majid Soomro[1], Sanaullah Jamali[3], Tarique Ali Siyal[1], Irfan Ali Sanjrani[1], Andleeb Soomro[1], Ramsha Saleem[1], Zaheer Ahmed Ujan[1] and Muhammad Aslam Khoso[1]

[1]Institute of Physics, University of Sindh, Jamshoro 71000, Pakistan

[2]Anhui Provincial Key Laboratory of Photonic Devices and Materials, Anhui Institute of Optics and Fine Mechanics, Hefei Institutes of Physical Sciences, Chinese Academy of Sciences, Hefei 230031, China

[3]University of Sindh, Laar Campus @ Badin, 72200, Pakistan

Corresponding Author email: saifjamali86@yahoo.com

Abstract

Laser-induced breakdown spectroscopy (LIBS) was employed for simultaneous elemental profiling and plasma diagnostics of commercially available cosmetic products (face blusher and eyeshadow), motivated by growing concerns about toxic metal contamination and associated health risks, including skin irritation, neurological disorders, and carcinogenic effects. Plasma was generated under ambient conditions at atmospheric pressure in air using a Q-switched Nd: YAG laser (532 nm, 5 ns pulse duration, 10 Hz repetition rate). Emission spectra were recorded in the 200–720 nm range, enabling the detection of major and trace elements including Ca, Ti, Mn, Cu, Hg, Cr, Li, Ba, Pb, Na, Fe, Al, and Mg. To ensure reproducibility, spectra were averaged over multiple laser shots at different spatial locations on each sample. Spatially resolved plasma diagnostics were performed to investigate the dynamics of laser–matter interactions. The electron temperature, determined using the Boltzmann plot method under local thermodynamic equilibrium (LTE), decreased from 14,151 K to 5,465 K for sample A and from 13,302 K to 4,157 K for sample B with increasing axial distance. Electron number density, estimated via Stark broadening, ranged from 6.08×10^{16} to 1.24×10^{16} cm^{-3} and 1.03×10^{17} to 1.98×10^{16} cm^{-3}, respectively, consistent with typical LIBS plasma conditions. Moreover, inverse bremsstrahlung absorption and the plasma frequency were evaluated to understand plasma evolution and energy-coupling mechanisms. The presence of toxic elements such as Pb and Hg emphasizes potential health risks and highlights the importance of rapid screening techniques. The results demonstrate that LIBS is a reliable, rapid, and non-destructive technique for cosmetic safety assessment and quality control.

Keywords: LIBS; Plasma diagnostics; Cosmetic analysis; Electron temperature; Electron density

1. Introduction

Laser-Induced Breakdown Spectroscopy (LIBS) is an emission-based analytical technique in which a high-energy laser pulse interacts with a material, generating a microplasma whose emission spectrum reveals the elemental composition [1-4]. The performance of LIBS depends on laser parameters, sample properties, and ambient conditions [5-6]. LIBS has been widely applied in environmental monitoring [7-8], welding monitoring [9], plastic analysis [10], chemical analysis [11], and industrial and security applications [12].

Several studies have reported the detection of toxic metals in cosmetics using spectroscopic techniques. For example, Lara-Torres et al. [13] determined the Presence of Lead (Pb) and Cadmium (Cd) in lipstick samples. Ahmed et al. [14] studied lipstick using LIBS and found Lead (Pb), Chromium (Cr), Cadmium (Cd), and Zinc (Zn). Rehan et al. [15] detect Lead (Pb) in fresh henna leaves and cultivated soils using LIBS. Ahmed et al. [16] estimated the concentration of Silicon (Si), Magnesium (Mg), Titanium (Ti), Aluminum (Al), Barium (Ba), Zinc (Zn), Chlorine (Cl), and Rubidium (Rb) in Blusher components for unbranded cosmetic brands using X-ray fluorescence and LIBS techniques. Nourmoradi et al. [17] estimated the concentration of Lead (Pb) and Cadmium (Cd) in the lipsticks in the range of (0.08 – 5.2) µg/g and (4.08 – 60.20) µg/g, for eye shadow, the concentration of Lead (Pb) and Cadmium (Cd) ranges from (0.85 – 6.90) µg/g and (1.54 – 55.59) µg/g. Al-azawi et al. [18] estimated the concentration of Lead (Pb) and Chromium (Cr) in the range of (0.10 – 4.85) ppm and (0.18 – 5.2) ppm in Iraqi lipsticks using Atomic Absorption Spectroscopy (AAS). Świerczek et al. [19] determined the heavy metals in Chinese eye shadow using atomic absorption spectrometry (AAS) and found Zinc (Zn), Nickel (Ni), Cadmium (Cd), Copper (Cu), and Lead (Pb). Laghari et al. [20] reported Aluminum (Al), Barium (Ba), Calcium (Ca), Chromium (Cr), Copper (Cu), Lead (Pb), Potassium (K), Lithium (Li), Magnesium (Mg), Sodium (Na), Titanium (Ti), Zinc (Zn), and Hydrogen (H) in face blusher power sample.

Although similar cosmetic products have been investigated in previous studies, variations among manufacturers can lead to significant differences in composition and spectral response. Therefore, the present study focuses on the comparative analysis of cosmetic samples from different companies using a real-time atomic emission spectroscopic technique. This approach integrates elemental profiling with comprehensive plasma characterization, including electron temperature, electron number density, plasma frequency, and other related plasma parameters. It provides deeper insight into plasma evolution and enhances the reliability of LIBS for cosmetic analysis.

2.0. Materials and Methods

2.1 Sampling Collection and Preparation

The cosmetic product names, Face Blusher (coded as A) and Eye Shadow (coded as B), were obtained from cosmetic stores in Hyderabad, Pakistan. The sample was heated to 100 °C to remove any excess water contamination, then frozen and cut into little circular pieces of 1 cm diameter to fit into the sample disk holder. The experimental setup (Fig. 1) used Second Harmonic Generation (SHG) at 532 nm from a Q-switched Nd:YAG (Quantel Brilliant) laser with a pulse length of 5 ns and a repetition rate of 10 Hz. The laser is capable of producing up to 200 mJ of energy per pulse at 532 nm. The laser beam was focused on the target in the air at atmospheric pressure using 20 cm quartz lens. To prevent cratering, each emission spectrum was captured on a clean surface. The emission spectrum from the plasma was recorded with the LIBS2000 (Ocean Optics, Inc.) detection device, in conjunction with an optical fiber (high OH, core diameter: 600 µm, collimating lens with 0 –45° field of view) positioned at right angles to the direction of plasma expansion. The LIBS2000 detection system has five spectrometers, each with a 5 µm slit width, and the total wavelength range of all five HR spectrometers are 200 to 720 nm. Each spectrometer features a linear CCD array with a resolution of 2048 elements and an optical resolution of 0.1 nm. Through a four-channel digital delay/pulse generator. The LIBS2000 detection system and the Nd:YAG laser were synchronized via a delay generator (SRS DG535). Data from all five spectrometers were collected simultaneously and saved on a PC using the OOI LIBS software for further processing.

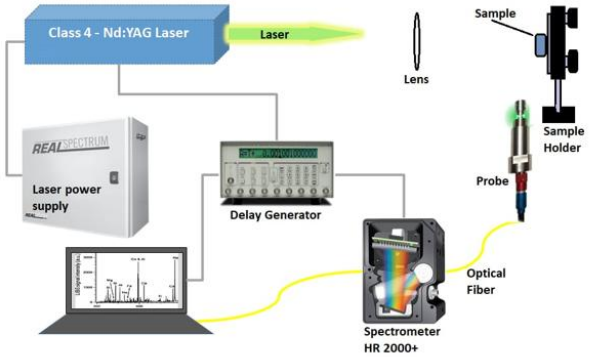

Figure 1: LIBS Experimental Setup [2].

3.0. Results and Discussion

3.1 The atomic emission spectrum of laser-produced plasma

The emission spectra of laser-produced plasma revealed the presence of Ca, Ti, Mn, Cu, Hg, Cr, Li, Ba, Pb, Na, Fe, Al, and Mg in both samples. The complete emission spectrum is divided into small portions for better presentation, and the individual transition lines (Fig. 2a-k). The reported emission lines and their corresponding wavelengths are given in Table 1.

Table 1: Transition lines of trace elements in the laser-produced plasma of the cosmetic sample.

Elements	Transition lines (nm)
Ca	393.36, 396.84, 422.67, 428.30, 428.93, 429.89, 430.25, 430.77, 431.50, 431.86, 442.54, 443.49, 445.47, 519.02, 526.17, 526.42, 526.54, 551.29, 558.19, 558.87, 559.45, 559.84, 560.28, 585.74, 610.27, 612.22, 616.21, 616.95, 643.91, 644.98, 646.25, 646.25, 649.37, 714.81
Ti	332.27, 332.97, 334.18, 334.94, 336.11, 337.28, 338.37, 339.47, 394.86, 395.82, 398.17, 398.97, 399.86, 401.96, 439.50, 451.27, 451.80, 452.27, 452.73, 453.55, 454.46, 454.96, 457.19, 461.95, 462.30, 463.78, 464.04, 464.51, 465.60, 466.75, 468.19, 469.36, 469.87, 471.01, 472.31, 474.27, 476.63, 498.17, 499.10, 499.95, 500.72, 501.42, 503.64, 506.46
Mn	403.07
Cu	515.32, 521.82
Hg	404.65
Cr	520.84
Li	670.77
Ba	455.40, 493.40, 553.54, 611.07, 614.17, 652.73, 659.53, 667.52, 669.38, 705.99
Pb	405.78, 520.14
Na	588.99, 589.59
Fe	388.62, 407.17, 408.36, 432.57, 438.35, 440.47, 492.05
Al	394.40, 396.15
Mg	382.93, 383.23, 383.82, 516.73, 517.26, 518.36

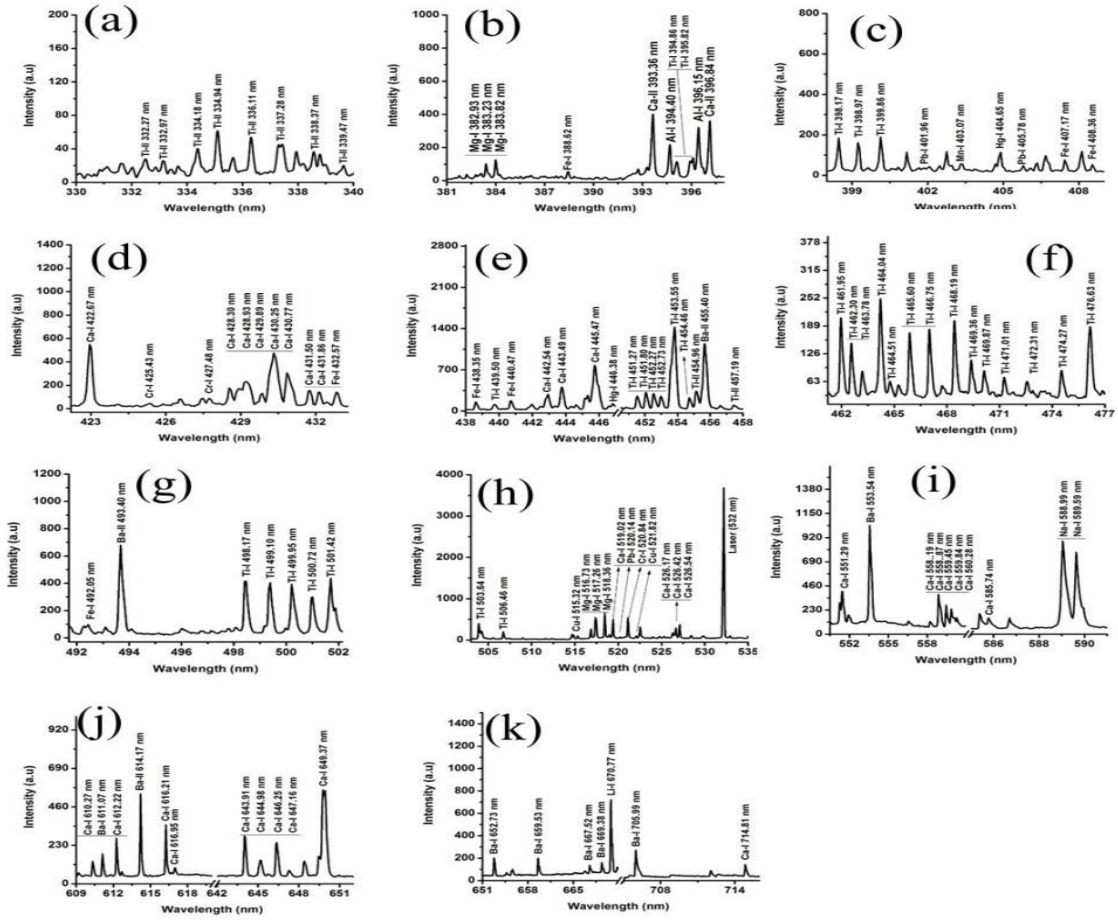

Figure 2: (a-k): LIBS emission spectra of laser-produced spectra of cosmetic agents.

To study the hydrodynamic variations in the emission lines of laser-produced plasma at different distances, we have recorded the emission spectrum at different positions along the plasma's axial direction during expansion. It was observed that the plasma near the sample surface is denser and emits more strongly. The plasma density and line intensity decreased with increasing distance from the plasma surface. This variation may be due to thermalization and recombination in the plasma. The spatial variation in the Intensity of the transition line of Magnesium triplet at 382.93 nm, 383.23 nm, 383.82 nm, variation in the Calcium triplet at 526.17 nm, 526.42 nm and 526.54 nm, and variation in the Intensity of the Sodium doublet transition lines at 588.99 nm and 589.59 nm (Fig. 3a-c).

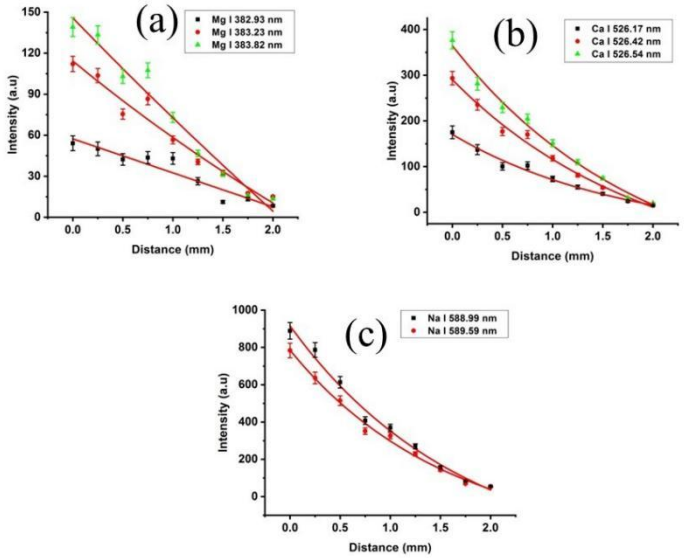

Figure 3(a-c): Intensity variation of Magnesium (Mg), Calcium (Ca), and Sodium (Na) with distance (0 – 2) mm.

This variation is also reproduced in the three-dimensional graph of Intensity, width, and spatial distance (Fig. 4 a-c). We have calculated the integrated intensity ratio of the transition lines of the triplets of Magnesium (Mg) and Calcium (Ca), and doublet of Sodium (Na) reported as the Magnesium triplet (382.93 nm/383.23 nm = 0.40, 383.23 nm / 383.82 nm =

0.80 and 382.93 nm / 383.82 nm = 0.32) Calcium triplet (526.17 nm / 526.42 nm = 0.59, 526.42 nm / 526.54 nm = 0.78 and 526.17 nm / 526.54 nm = 0.46) and the Sodium doublet (588.99 nm / 589.59 nm = 1.13).

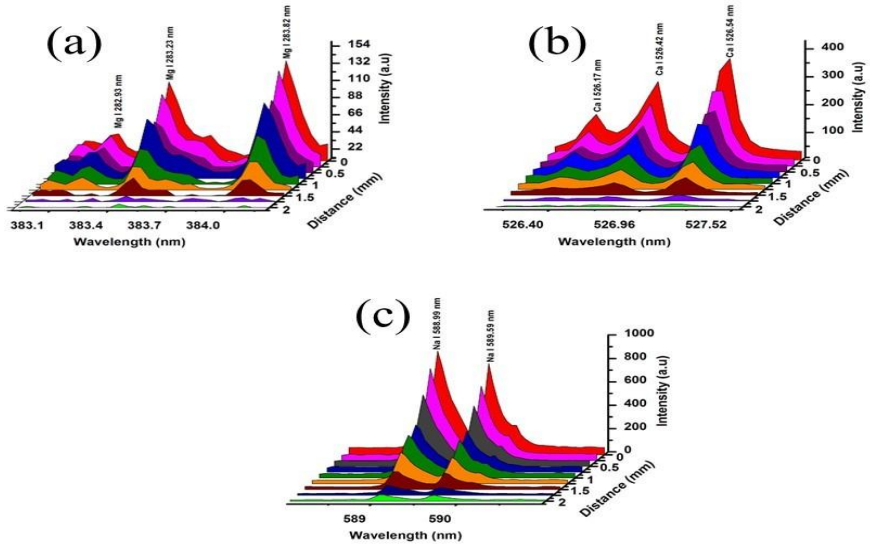

Figure 4 (a-c): 3D intensity and width variation of Mg, Ca, and Na with distance (0 – 2) mm.

3.2 Spatially Resolved Plasma Diagnostics

The electron temperature of a laser-produced plasma is an essential metric for investigating the complex phenomena that occur in plasma. The computation of electron temperature provides data on the ionization and excitation processes that occur in plasma. We have determined the electron temperature using the Boltzmann Plot Method under the assumption of the local thermodynamic equilibrium (LTE). In these calculations, we used the integrated Intensity of the neutral transition lines of Ca at (442.54, 443.49, 445.47, 644.98, 646.25, and 649.37) nm.

Boltzmann plot Method under the condition of LTE is given by Eq. (1) [21].

$$ln\left(\frac{\lambda_{ji}I_{ji}}{A_{ji}g_j}\right) = ln\left(\frac{N}{Z}\right) - \left(\frac{E_j}{kT_e}\right) \quad (1)$$

Where, λ_{ji} is the wavelength of the transition lines, I_{ji} is the integrated signal intensity, A_{ji} is the transition probability, g_j is the statistical weight, N is the upper-level population, Z is the partition function, E_j is the upper energy, k is the Boltzmann constant, and T_e is the electron temperature.. The graph of $ln\left(\frac{\lambda_{ji}I_{ji}}{A_{ji}g_j}\right)$ vs E_k shows a straight line with a slope of $\left(-\frac{1}{KT_e}\right)$. The spatial variation of the electron temperature was estimated as (14151 – 5465) K for sample A, and for sample B, it varies as (13302 – 4157) K with the distance from (0 – 2) mm along the axial direction. The variation in electron temperature with distance (Fig. 5a). It was noticed that the electron temperature of both samples decreases exponentially with distance. The electron number density was estimated using the Stark-broadened line-profile method. The electron number density of the plasma was estimated using the relation given in (Eq. 2) [22].

$$\Delta\lambda_{FWHM} = 2w\left(\frac{N_e}{10^{16}}\right) \quad (2)$$

Where, N_e is the electron number density and $\Delta\lambda_{FWHM}$ is the Full-Width Half Maximum of the wavelength of the transition line. The FWHM of the line at 393.36 nm was determined from a Lorentzian fit to the transition line. The determined value of FWHM is 0.231 nm (Fig. 5b). The estimated value of electron number density varies as (6.08×10^{16} – 1.24×10^{16}) cm^{-3} for sample A plasma and for sample B plasma, it varies from (1.03×10^{17} – 1.98×10^{16}) cm^{-3} with distance from (0- 2) mm. The variation of electron number density(Fig. 5c). It was observed that the electron number density in both plasmas decreases exponentially with distance. At the initial stage, the plasma is hot and dense; both plasma properties decrease due to thermalization and recombination. In this laser-produced plasma, the three-body recombination process appears to be more dominant than radiative recombination.

In the nanosecond laser-matter interaction, the plasma is generated in the femtosecond time; therefore, the rest of the nanosecond laser pulse is absorbed in the plasma via (Inverse Bremsstrahlung and photoionization process) that causes further heating and ionization of the plasma. The Inverse Bremsstrahlung process is dominant for long-wavelength (Infrared) lasers, while photoionization is dominant for short-wavelength (Ultraviolet) lasers. We have estimated the inverse bremsstrahlung coefficient using the relation (Eq. 3) [23].

$$\alpha_{ib} = 1.37 \times 10^{-35}\, \lambda^3 \frac{{N_e}^2}{\sqrt{T_e}} \quad (3)$$

Where, α_{ib} is the inverse bremsstrahlung coefficient, λ is the laser wavelength, T_e is the electron temperature, and N_e is the electron number density. The estimated value of the inverse bremsstrahlung coefficient for both samples varies as $(6.41\times10^{-5} - 4.30\times10^{-6})$ cm^{-1} and $(1.90\times10^{-4} - 1.27\times10^{-5})$ cm^{-1} with the distance from (0-2) mm, respectively (Fig. 5d).

The species in the plasma plume oscillate at a high frequency due to the temperature and the electrostatic field during laser-matter interaction, and this frequency is called the plasma frequency. Plasma frequency affects laser beam reflection and absorption. The plasma frequency was calculated using Equation (4) [24].

$$\upsilon_P = 9 \times 10^3 \sqrt{N_e} \quad (4)$$

where, N_e is the electron number density, and υ_P is the plasma frequency. The maximum plasma frequencies of 2.22×10^{12} Hz for sample A and 2.89×10^{12} Hz for sample B at a 0 mm distance have been calculated. Because most of the laser energy absorbed in plasma may induce mass ablation, the plasma frequency is less than the laser frequency (4.08×10^{14} Hz) at 532 nm wavelength. The variation of plasma frequency at a distance (0 – 2) mm was found as $(2.22 - 1.01)\times10^{12}$ Hz for sample A and $(2.89 - 1.27)\times10^{12}$ Hz for sample B (Fig. 5e).

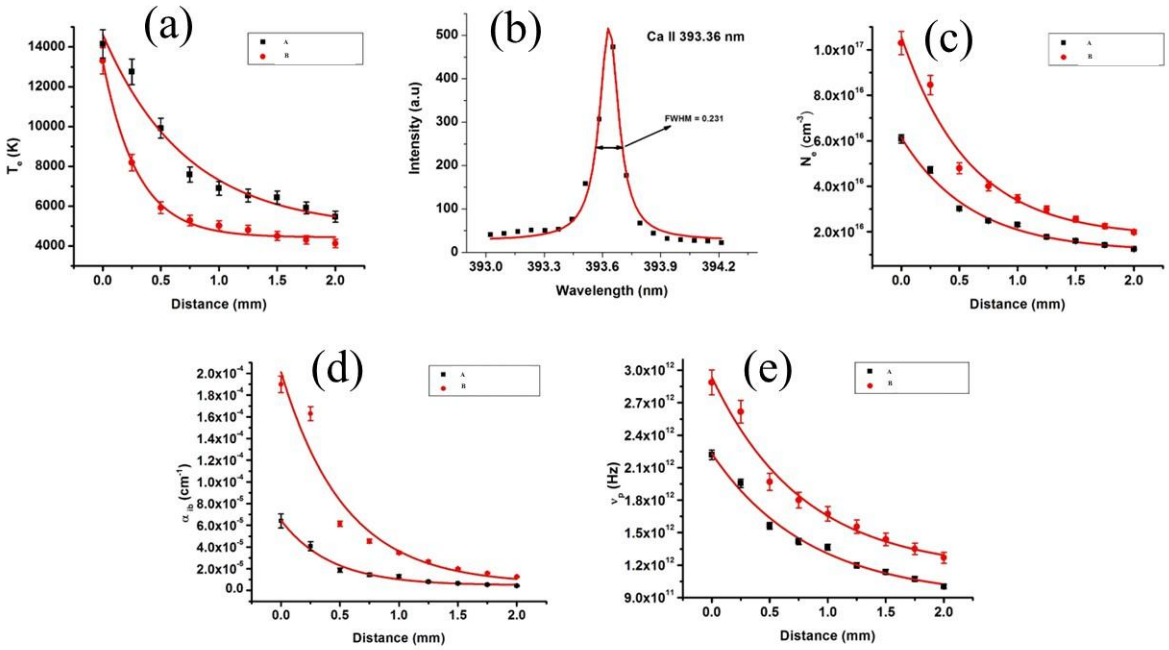

Figure 5: Variation of (a) electron temperature, (b) Calcium (Ca) ionic line at 393.36 nm, the solid line represents the Lorentzian fit while dotted line shows actual data (c) electron number density (d) inverse bremsstrahlung co-efficient (e) plasma frequency of laser induced plasma with distance (0 – 2) mm.

4.0 Conclusion

The study concludes with novel findings from optical emission spectroscopy of laser-produced plasma. The elements Ca, Ti, Mn, Cu, Hg, Cr, Li, Ba, Pb, Na, Fe, Al, and Mg were detected, However in our previous work [20], we have reported Al, Ca, Cr, Cu, Pb, K, Li, Mg, Na, Ti, Zn, and H, indicating both consistency and additional elemental detection in the present study. The detection of potentially toxic elements such as Pb and Hg raises important concerns regarding the safety of cosmetic products. The intensity of all observed transition lines in sample A plasma is significantly higher than in sample B. Furthermore, the plasma temperature, calculated using the Boltzmann plot technique, ranges from 14,151 to 5,465 K for sample A plasma and from 13,302 to 4,157 K for sample B plasma. From Stark broadening line profiles, the electron number density was determined to be $(6.08\times10^{16} - 1.24\times10^{16})$ cm^{-3} for face blusher (sample A) and $(1.03\times10^{17} - 1.98\times10^{16})$ cm^{-3} for sample B plasma. Sample A exhibits a plasma frequency in the range of $(2.22 - 1.01)\times10^{12}$ Hz, whereas sample B shows a plasma frequency of $(2.89 - 1.27)\times10^{12}$ Hz. The inverse bremsstrahlung coefficient for samples A and B varies from $(6.41\times10^{-5} - 4.30\times10^{-6})$ cm^{-1} and $(1.90\times10^{-4} - 1.27\times10^{-5})$ cm^{-1}, respectively. Overall, the results demonstrate that LIBS is a rapid, non-destructive, and reliable technique for simultaneous elemental analysis and plasma diagnostics. The findings further confirm that manufacturer-dependent variations play a crucial role in influencing plasma characteristics and spectral behavior, highlighting the potential of LIBS for cosmetic safety assessment and quality control.

Acknowledgment

All Authors are thankful to Quaid-e-Azam University, Islamabad, for providing the necessary experimental facilities in the atomic and molecular physics laboratory.

Author's Contribution: S. Jamali (conceptualization, experiment, data analysis, writing—original draft), N. M. Shaikh (supervision, review and editing), Z. Zhang (validation), H. Fu (validation), W. A. Bhutto (validation), A. M.

Soomro (validation), S. Jamali (validation), T. A. Siyal (visualization), I. A. Sanjrani (visualization), A. Soomro (visualization), R. Saleem (visualization), Z. A. Ujan and M. A. Khoso (visualization).

Conflict of Interest: Authors has no conflict of interest.

Funding Resource: This research is supported by the Higher Education Commission (HEC) of Pakistan, through the National Research Program for Universities, NRPU Project #10166.

References

1. Zhao, S., Afgan, M. S., Zhu, H., & Gao, X. (2022). Femtosecond laser filamentation-induced breakdown spectroscopy combined with chemometric methods for soil heavy metals analysis. *Optik, 251*, 168444. https://doi.org/10.1016/j.ijleo.2021.168444
2. Jamali, S., Shaikh, N. M., Khoso, M. A., Jamil, Y., Bhutto, W. A., Soomro, A. M., & Mari, R. H. (2022). Elemental analysis of talcum powder using spectroscopic techniques. *Optik, 261*, 169246. https://doi.org/10.1016/j.ijleo.2022.169246
3. Song, X., Li, K., Dai, K., Wang, X., Du, H., & Zhao, H. (2022). A random-forest-assisted artificial neural network method for analysis of steel using laser-induced breakdown spectroscopy. *Optik, 249*, 168214. https://doi.org/10.1016/j.ijleo.2021.168214
4. Shaikh, N. M., Rashid, B., Hafeez, S., Jamil, Y., & Baig, M. A. (2006). Measurement of electron density and temperature of a laser-induced zinc plasma. *Journal of Physics D: Applied Physics, 39*, 1384–1391. https://doi.org/10.1088/0022-3727/39/7/008
5. Jamali, S., Khoso, M. A., Zaman, M. H., Jamil, Y., Bhutto, W. A., Abbas, A., Mari, R. H., Kalhoro, M. S., & Shaikh, N. M. (2021). Elemental analysis using laser ablation and atomic absorption spectroscopy (AAS) techniques. *Physica B: Condensed Matter, 620*, 413278. https://doi.org/10.1016/j.physb.2021.413278
6. Ashraf, M., Shaikh, N. M., Kandhro, G. A., Murtaza, G., Iqbal, J., Iqbal, A., & Lashari, S. A. (2020). Energy penetration and inverse bremsstrahlung absorption coefficient in laser-ablated germanium plasma. *Journal of Molecular Structure, 1203*, 127412. https://doi.org/10.1016/j.molstruc.2019.127412
7. Farooq, W. A., Al-Johani, A. S., Alsalhi, M. S., Tawfik, W., & Qindeel, R. (2020). Analysis of polystyrene and polycarbonate used in manufacturing of water and food containers using laser-induced breakdown spectroscopy. *Journal of Molecular Structure, 1201*, 127152. https://doi.org/10.1016/j.molstruc.2019.127152
8. Zhang, Y., Zhang, T., & Li, H. (2021). Application of laser-induced breakdown spectroscopy (LIBS) in environmental monitoring. *Spectrochimica Acta Part B: Atomic Spectroscopy, 181*, 106218. https://doi.org/10.1016/j.sab.2021.106218
9. Lednev, V. N., Sdvizhenskii, P. A., Stavertiy, A. Y., Grishin, M. Y., Tretyakov, R. S., Asyutin, R. D., & Pershin, S. M. (2021). Online and in situ laser-induced breakdown spectroscopy for laser welding monitoring. *Spectrochimica Acta Part B: Atomic Spectroscopy, 175*, 106032. https://doi.org/10.1016/j.sab.2020.106032
10. Zeng, Q., Sirven, J. B., Gabriel, J. C. P., Tay, C. Y., & Lee, J. M. (2021). Laser-induced breakdown spectroscopy for plastic analysis. *TrAC Trends in Analytical Chemistry, 140*, 116280. https://doi.org/10.1016/j.trac.2021.116280
11. Novel LIBS method for micro-spatial chemical analysis of inorganic gunshot residues. (n.d.). Retrieved September 8, 2021, from https://analyticalsciencejournals.onlinelibrary.wiley.com/doi/epdf/10.1002/cem.3208
12. Bol'shakov, A. A., Yoo, J. H., Liu, C., Plumer, J. R., & Russo, R. E. (2010). Laser-induced breakdown spectroscopy in industrial and security applications. *Applied Optics, 49*, C132–C142. https://doi.org/10.1364/AO.49.00C132
13. Lara-Torres, S., Figueiredo, D., Paz, S., Gutiérrez, A. J., Rubio, C., González-Weller, D., Revert, C., & Hardisson, A. (2021). Determination and risk assessment of toxic metals in lipsticks from Europe and China. *Journal of Trace Elements in Medicine and Biology, 67*, 126792. https://doi.org/10.1016/j.jtemb.2021.126792
14. Ahmed, A. E. (2017). Elements tracing of lipsticks using laser-induced breakdown spectroscopy. *[Journal Name], 106*, 46802–46805.

15. Rehan, I., Gondal, M. A., Rehan, K., Sultana, S., Dastageer, M. A., & Al-Adel, F. F. (2019). LIBS for the detection of lead in ready-to-use henna paste and nutrients in fresh henna leaves and cultivated soils. *Talanta, 199*, 203–211. https://doi.org/10.1016/j.talanta.2019.02.047
16. Ahmed, A., Salman, M., Alwazzan, M., & Meri, A. (2019). Blushers component analysis for unbranded cosmetic brands: Elements' concentration levels and its effect on human body. *Journal of Advanced Research in Dynamical and Control Systems, 11*, 412–419.
17. Nourmoradi, H., Foroghi, M., Farhadkhani, M., & Dastjerdi, M. V. (2013). Assessment of lead and cadmium levels in frequently used cosmetic products in Iran. *Journal of Environmental and Public Health, 2013*, 962727. https://doi.org/10.1155/2013/962727
18. Al-Azawi, K. F., Al-Gebori, A. M., Obayes, H. R., & Khasraghi, A. H. (2018). Levels of lead and chromium ions in different brands of lipstick sold at local markets in Iraq. *Engineering and Technology Journal, 36*, 147–151. https://doi.org/10.30684/etj.36.2b.9
19. Świerczek, L., Cieślik, B., Matysiak, A., & Konieczka, P. (2019). Determination of heavy metals in eyeshadows from China. *Monatshefte für Chemie, 150*, 1675–1680.
20. Laghari, A., Shaikh, N. M., Bhutto, W. A., Soomro, A. M., Jamali, S., Khoso, M. A., Sanjrani, I. A., Arain, Z. H., & Laghari, N. M. (n.d.). Elemental analysis of face blusher powder using laser-induced breakdown spectroscopy. *Pakistan Journal of Chemistry, 15*(4), 132–137.
21. Hanif, M., & Salik, M. (2018). Emission studies of silicon plasma produced by a Nd:YAG laser. *Silicon, 10*, 1067–1075.
22. Khoso, M. A., Shaikh, N. M., Kalhoro, M. S., Jamali, S., Ujan, Z. A., & Ali, R. (2022). Comparative elemental analysis of soil of wheat, corn, rice, and okra cropped field using CF-LIBS. *Optik, 261*, 169247. https://doi.org/10.1016/j.ijleo.2022.169247
23. Jamali, S., Bhutto, W. A., Nizamani, A. H., Saleem, H., Khaskheli, A., Soomro, A. M., Sahito, A. G., Shaikh, N. M., & Saleem, S. (2019). Spectroscopic analysis of lithium fluoride (LiF) using laser ablation. *International Journal of Computer Science and Network Security, 19*, 127.
24. Rehan, I., Rehan, K., Sultana, S., Oun Ul Haq, M., Niazi, M. Z. K., & Muhammad, R. (2016). Spatial characterization of red and white skin potatoes using nanosecond laser-induced breakdown in air. *EPJ Applied Physics, 73*, 1–8. https://doi.org/10.1051/epjap/2015150453

Received: February 26th 2026 **Accepted: March 31st 2026**